2013 IEEE/ASME International Conference on
Advanced Intelligent Mechatronics (AIM)
Wollongong, Australia, July 9-12, 2013

An Analysis of Homeostatic Motion Control System for a Hybrid-Driven Underwater Glider*

Khalid Isa, and M.R. Arshad, *Member, IEEE*

***Abstract*— This paper presents an analysis of homeostatic controller, which controls the motion of a hybrid-driven underwater glider. The homeostatic controller is inspired from a biological process known as homeostasis, which maintains a stable state in the face of massively dynamics conditions. Within a biological context, organism homeostasis is an emergent property of the interactions between nervous, endocrine and immune system. Artificially these three systems are presented as Artificial Neural Network (ANN), Artificial Endocrine System (AES) and Artificial Immune System (AIS). The ANN is designed as the controller backbone, the AES is designed as the weight tuner, and the AIS is designed as the optimizer of the control system. The design objective is to obtain better control performance of the motion control system which includes the disturbance from the water currents. We have simulated the algorithm by using Matlab™, and the results demonstrated that the homeostatic controller reduced the cost function of the control system and produced better control performance than the neuroendocrine controller.**

I. Introduction

The classical and modern control systems have been implemented to control autonomous underwater vehicle (AUV) and underwater glider, and have shown weaknesses under dynamic changing environments. Numerous underwater glider control systems have been proposed by previous researchers. Most existing gliders have used the PID and LQR controller to control the motion and attitude [1-6]. The sliding mode control (SMC) also has been used to control the underwater glider [7-8], but the main constraint in SMC is the chattering effect, which can degrade the performance of the system, and make the system unstable. Although these controller methods have already demonstrated acceptable results, the control system is considered as the Single-Input-Single Output (SISO) system. Thus, they still have limitations in terms of control performance for the Multiple-Input-Multiple-Output (MIMO) system. Since the hybrid-driven glider model is very complex and has MIMO system, it is difficult to control the glider. In addition, the high nonlinearity of the glider dynamics and underwater disturbances are also the main reasons that make the glider difficult to control [9-10].

*Research supported by Malaysia Ministry of Higher Education (MOHE), ERGS-203/PELECT/6730045, Universiti Sains Malaysia (USM), and Universiti Tun Hussein Onn Malaysia (UTHM).

Khalid Isa is with the Underwater Robotics Research Group (URRG) and Department of Computer Engineering, Faculty of Electrical and Electronic Engineering, Universiti Tun Hussein Onn Malaysia (UTHM), 86400 Parit Raja, Batu Pahat, Johor, Malaysia (+6012-7732488; fax: +604-5941023; e-mail: halid@uthm.edu.my or isa.khalid@yahoo.com).

M. R. Arshad is with Underwater Robotics Research Group (URRG), School of Electrical and Electronic Engineering, Engineering Campus, Universiti Sains Malaysia (USM), 14300 Nibong Tebal, Pulau Pinang, Malaysia (e-mail: rizal@eng.usm.my).

Due to that, the gliders should be truly autonomous which operate steadily and adaptively to their environment. Therefore, the biologically inspired control systems should be considered because they are autonomous and adaptive in nature. One possible approach is come from biology process, which known as homeostasis, which maintains a stable state in the face of massively changing conditions. Conceptually, this biological process has inspired and motivated applications of homeostasis in the synthesis of autonomous systems in mobile robotics as presented in [11-15]. However, until now, the effectiveness of the homeostatic controller on underwater platform such as the AUV or glider has not been investigated. Due to that, we have designed the homeostatic controller for the glider motion control.

The homeostatic control mechanism is a connectionist of ANN, AES and AIS. These three systems do not act in isolation; instead they are a single system that control the motion of the glider. Thus, in order to design the controller, we have designed a neural network predictive control for the hybrid-driven underwater glider [16]. However, in order to overcome the weight tuning problem due to the presence of disturbance from the water current, we have added an artificial gland cell of AES as a weight tuning factor for the network. Then, the AIS is used as an optimizer to the motion control system, which based on the clonal selection algorithm (CSA).

The objective of this work is to analyse the performance of the homeostatic controller by comparing with the neuroendocrine controller. We have analysed the homeostatic controller with the LQR, Model Predictive Controller (MPC), and Neural Network Predictive Controller (NNPC). However, in this paper, the neuroendocrine is selected for the comparison because of the necessity to observe the significant improvement in terms of controller's performance after the tuning and optimisation. This paper is organized as follows. Section II presents the equations of motion of the hybrid-driven glider. The implementation of the homeostatic controller is explained in Section III. Section IV describes the simulation results. Finally, the conclusion is given in Section V.

II. Hybrid-Driven Underwater Glider

Technically, the USM hybrid-driven underwater glider integrates the features of a buoyancy-driven underwater glider and a typical or propeller-driven AUV. In addition, instead of using fixed wings like the existing glider, we have modeled and designed the glider with wings and a rudder that can be controlled independently. The main reason to design the hybrid-driven glider is to overcome the speed and maneuverability limitations of the buoyancy-driven glider. Although, the hybrid-driven glider will be used more energy

than the buoyancy-driven glider, it would reduce the gap between energy consumption, speed and maneuverability of the glider.

Due to that, the hybrid-driven underwater glider can be propelled by using buoyancy and/or propulsion system. The glider has a ballast pump to control the depth, an internal sliding mass to control the pitch angle during gliding, wings and a rudder to control the roll and yaw angle for turning motion. Therefore, by efficiently managing the driving mode of the glider, the energy from the power system can be used efficiently. For example, if the glider is set for a long duration mission that required a straight line gliding mode, only the ballast and internal moving mass will be activated, and if the glider is set for a hovering mission, the propeller will be activated, and the external actuators will be activated. Fig. 1 shows the Solidworks™ drawing of the glider.

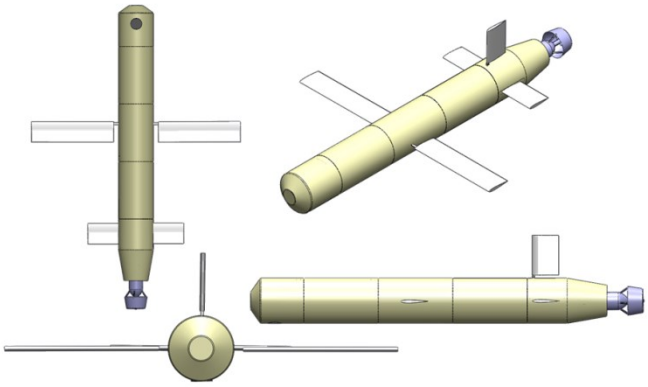

Figure 1. Glider structure from back, trimetric, front and right view.

In order to analyze the glider motion, the nonlinear equation of motion for the hybrid-driven underwater glider is written as:

$$\dot{\eta} = [\dot{x}, \dot{y}, \dot{z}, \dot{\emptyset}, \dot{\theta}, \dot{\psi}] = J(\eta)V \text{ and} \quad (1)$$

$$\dot{V} = [\dot{u}, \dot{v}, \dot{w}, \dot{p}, \dot{q}, \dot{r}] = \dot{V}_c + M^{-1}(-C(V) - D(V_r, \delta) - g(\eta) - P) \quad (2)$$

where $J(\eta)$ is the rotation and transformation matrix of the Euler angles, V is the translational and rotational velocity, V_c is the current velocity, V_r represents the relative velocity, M represents the system inertia matrix of the glider, $C(V)$ represents the Coriolis-centripetal of the glider, $D(V_r, \delta)$ is the damping forces and moments, $g(\eta)$ is the gravitational and buoyancy forces and moments, and P represents the propeller forces. The notation of δ represents the deflection angle of the external actuators (wings and rudder). Thus, the deflection angles are defined as:

$$\delta = [\delta_{rw}, \delta_{lw}, \delta_r]^T \quad (3)$$

where δ_{rw}, δ_{lw} and δ_r are the deflection angles of the right wing, left wing and rudder, respectively.

In order to control the pitch angle of the glider through the internal sliding mass as well as propels the glider by using buoyancy, the parameter of $\dot{q}$ in the equations (2) need to be rewritten. Thus, the following equations which represent the effects of the sliding mass on $\dot{q}$ is included in the equation of motion.

$$\dot{q} = \frac{1}{J_2}((M_3 - M_1)uw - (r_{px}p_{px} + r_{pz}p_{pz})q - m_p g(r_{px}cos\theta + r_{pz}sin\theta) + M_{DL} - r_{pz}u_x + r_{px}u_z), \quad (4)$$

$$\dot{r}_{px} = \frac{1}{m_p}p_{px} - u - r_{pz}q, \quad (5)$$

$$\dot{r}_{pz} = \frac{1}{m_p}p_{pz} - w + r_{px}q, \quad (6)$$

$$\dot{p}_{px} = u_x, \quad (7)$$

$$\dot{p}_{pz} = u_z, \text{ and} \quad (8)$$

$$\dot{m}_b = u_b \quad (9)$$

where J_2 represents the second element of the system inertia matrix, M_1 and M_3 are the element of the system mass matrix, m_p is the internal sliding mass, r_{px} and r_{pz} are the position of sliding mass in the x and z-direction, p_{px} and p_{pz} represent the force of sliding mass in the x and z-direction, m_b is the ballast pump mass, and M_{DL} is the viscous moment. The u_x, u_z and u_b represent the net force acting on the sliding mass in x-direction, the net force acting on the sliding mass in z-direction and the ballast pumping rate, respectively.

In order to control the glider's motion, we have defined 10 input parameters, which included 3 parameters of the water current velocity as disturbance. Thus, the 10 control inputs are denoted as:

$$u = [\delta_{rw}, \delta_{lw}, \delta_r, u_x, u_z, u_b, P_x, V_{cx}, V_{cy}, V_{cz}]^T \quad (10)$$

where the propeller force in x-direction is denoted as P_x. Lastly, the V_{cx}, V_{cy} and V_{cz} are the water current velocity in x, y and z direction, respectively.

In terms of the glider output, there are 17 outputs that represent the glider motion and attitude. Thus, the outputs are defined as:

$$y = [x, y, z, \emptyset, \theta, \psi, u, v, w, p, q, r, r_{px}, r_{pz}, P_{px}, P_{pz}, m_b]^T \quad (11)$$

where x, y and z are the position. The Euler angles are denoted as $\emptyset, \theta$ and ψ. The translational velocities are denoted as u, v and w. The p, q and r represent the angular velocities. The m_b is the ballast pump mass.

III. Implementation of Homeostatic Controller

The homeostatic controller is a combination of ANN, AES, and AIS which has the ability to alter the weights of the neural networks and optimize the control system. The neural network is the backbone of the controller, which predicts the control inputs, and outputs as well as achieving the target outputs. The endocrine system is the weight tuner of the neural network, which depending on the presence of disturbance from the water currents and also the level of sensitivity of the neural network weights. Meanwhile, the immune system based on the clonal selection algorithm (CSA) acts as the optimizer for the controller. Fig. 2 shows the homeostatic control system block diagram for the glider.

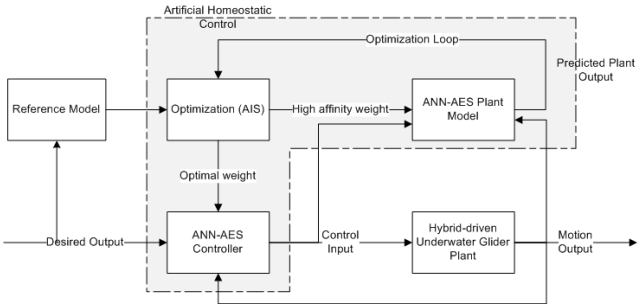

Figure 2. Homeostatic control system of the glider's motion

A. *The Neural Network Predictive Controller (NNPC)*

The objective of designing this controller is to map the desired control inputs for the glider plant as well as achieving the target outputs of the glider motion from the reference model. It also has the ability to handle the Multiple-Input-Multiple-Output (MIMO) system of the glider plant. In order to design the network models, the nonlinear plant of the glider must be linearized. The linearization is carried out to obtain the state-space representation of the Multiple-Input-Multiple-Output (MIMO) system of the glider.

The NNPC has two network models: the forward model, also known as the neural network plant model, and the inverse model, also known as the neural network controller. The MLP architecture for the NN forward model has 3 layers network with 10 control inputs (matrix B of the state space) as the input nodes, 10 hidden layer nodes, and 17 control outputs (matrix A of the state space) as the output nodes. We used the gradient descent with momentum and adaptive learning rate backpropagation as the training algorithm. The sigmoid transfer function in the hidden and output layer is used to estimate the output.

Generally, the activation function of the neuron in the NNPC is defined as:

$$a = \sum_i x_i w_i + b \tag{12}$$

where x_i is the input node values, and w_i is the weight. Thus, by introducing the AES as the weight tuner of the network, this equation has been rewritten in equation (13), which shows the new activation function that dependent on the hormone concentration and the sensitivity of the neuron to the hormone.

B. *The Artificial Endocrine System (AES)*

The AES is used to tune the weight of the NNPC in order to compensate with the disturbance. In line with the mechanism in the biological endocrine system, the AES have two major components: glands and hormones. The artificial endocrine gland, g, secretes an artificial hormone when they are stimulated by certain factors either external or internal stimuli. This artificial hormone can only effect the artificial hormones based on certain condition. In this work, the gland releases the hormone when the sensitivity of the NNPC's weight is lower than zero or the disturbance from the water current (velocity of the water current) is greater than zero.

In a biological endocrine system, not all artificial hormones must affect every neuron; it depends on the sensitivity of the neuron to the hormone, S_{ig} . However, in this work, we have assumed that every neuron are affected by the hormone with a constant value of the S_{ig}. Referring to [17], we include two main functions in the secretion of the endocrine gland: the stimulation rate of the gland, and the hormone concentration, G_{cg}. Thus, by using cooperative approach, we summed the multiplication of the w_i with G_{cg} and S_{ig}. Thus, the new activation function of the network namely the activation function of neuroendocrine networks is defined as:

$$a_{ne} = \sum_i x_i w_i \sum_g G_{cg} S_{ig} + b \tag{13}$$

The hormone concentration, G_{cg}, is defined as:

$$G_{cg}(t) = \beta_g G_{cg}(t) + S_{rg}(t) \tag{14}$$

where β_g is the decay rate of the hormone. In this work, β_g= 0.4. The value of hormone stimulation rate and decay rate is between a range of 0 to 1. The stimulation rate of the gland, S_{rg}, is defined as:

$$S_{rg}(t) = \frac{\alpha_g}{1+G_{cg}(t)} A_n(t) \tag{15}$$

where α_g is the hormone stimulation rate and A_n is the matrix A of the state-space from the neural network plant model. In this work, α_g= 0.9.

C. *The Artificial Immune System (AIS)*

In the late 1990s, the AIS has become popular among researchers. The theories, models, and applications of the AIS have been studied by Dasgupta [18], De Castro and Timmis [19] and Zheng et al. [20] have reviewed the AIS. The AIS can be utilized in two ways. Firstly, is to act as a growth regulator for cells within the artificial systems. In this case, the role of AIS is to remove cells, neurons, glands or connections that have a detrimental impact on the functioning of the system. Secondly, is to act as an optimizer of responding to the disturbances, which could be environmental changes that affect the ANN and AES. In this work, the AIS is used to optimize the weights of the neuroendocrine network.

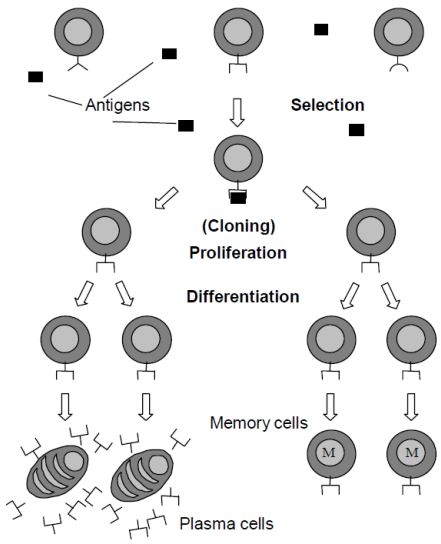

Figure 3. The principle of clonal selection [21]

In order to optimize the weights, we have designed the optimization algorithm based on the clonal selection mechanism. Biologically, the natural immune system used the clonal selection to define the basic response of the immune system to an antigenic stimulus. The idea of this theory is to proliferate the cells only if the cells able to recognize the antigens (Ag). As an example, when human is exposed to an antigen, the B lymphocytes cell in human's body respond by producing antibodies (Ab). Each cell releases only one antibody specifically to the antigen. Then, the antigen attach to the antibody, and with the signal from T-helper cell, the antigen stimulates the B cell to proliferate and mature into plasma cells. Fig. 3 shows the principle of the clonal selection in a biological system.

In this work, the CSA is formed to evolve the weight of the neuroendocrine network by means of selection, cloning, mutation and editing process. It was based on the CLONALG procedures that was proposed by De Castro and Von Zuben [22].

a) *Initialization:* Randomly initialize a population of the antibodies (Ab) based on the number of weights/antigens (Ag).

b) *Evaluation:* Compute all the affinity values for the Ab.

c) *Selection and Cloning:* Select the Ab values with a high affinity and generate the clones of the Ab proportionally to their affinity with the Ag.

d) *Mutation:* Mutate the clones inversely proportional to their affinity. Then, add these clones to the set of Ab and place a copy of the matured (optimized) Ab into the memory set.

e) *Editing:* Replace the lowest affinity Ab with a new randomly generated Ab.

f) *Repeat:* Repeat the process until the optimal weight achieved.

IV. Results and Analyses

The simulation was programmed by using Matlab™. We have simulated the control system with different values of desired Euler angles for 1200 seconds for gliding mode and hovering mode. However, in this paper, we only demonstrated the controller response for combination mode with two desired roll, pitch and yaw angles for 100 seconds. Thus, the desired roll angle, $\emptyset$, pitch angles θ, and yaw angle, ψ from the reference data for the first 50 seconds was set as 20^o, -35^o, and -15^o, and then -20^o, 35^o, and 15^o, respectively for another 50 seconds. The rest of the output parameters will be predicted by the controller, which is a response to the desired Euler angles.

The simulation results show the comparison of the glider motion between the neuroendocrine control response and homeostatic control response. We have simulated the controller response for a motion with and without disturbance from the water currents. However, in this paper, we only presented the response for both controllers for a motion with disturbance from the water currents. In this case, the velocity of the water current in the x-direction was set as 0.5 m/s.

Fig. 4 shows the comparison of the glider's position for the neuroendocrine response and homeostatic response according to the desired Euler angles that have been achieved. At the first 50 seconds, the graph demonstrated that the position of the glider for the neuroendocrine controller was determined as 2.96, 37.09, and 10.82 for $x, y,$ and z, respectively. Then, after the optimization process by the AIS in the homeostatic controller, the $x, y,$ and z position was determined as 13.65, -9.50, and 17.76, respectively. For the last 50 seconds, the glider's position for the neuroendocrine controller was determined as -2.96, -37.09, and -10.82 for $x, y,$ and z, respectively. On the other hand, the $x, y,$ and z position for the homeostatic controller was determined as -10.66, 5.7, and -18.86, respectively. From this observation, the value of the glider's position that was produced by the neuroendocrine controller is identical with a different direction for both periods, but for the homeostatic controller, due to the random population initialization of the Ab, the value of glider's position is different for both periods.

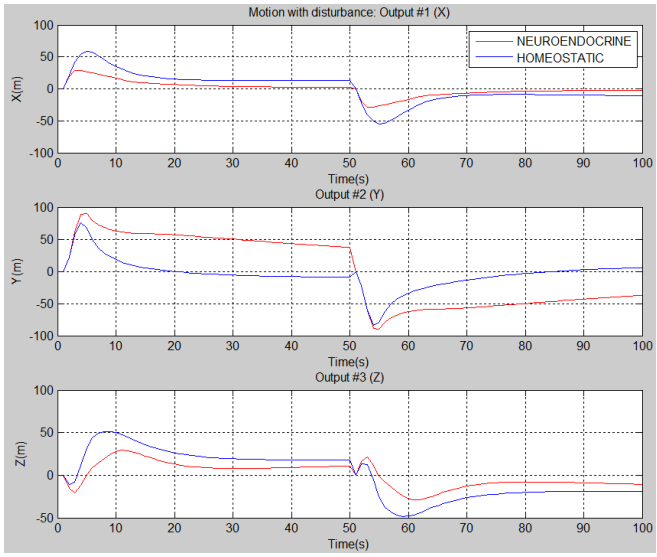

Figure 4. Glider position

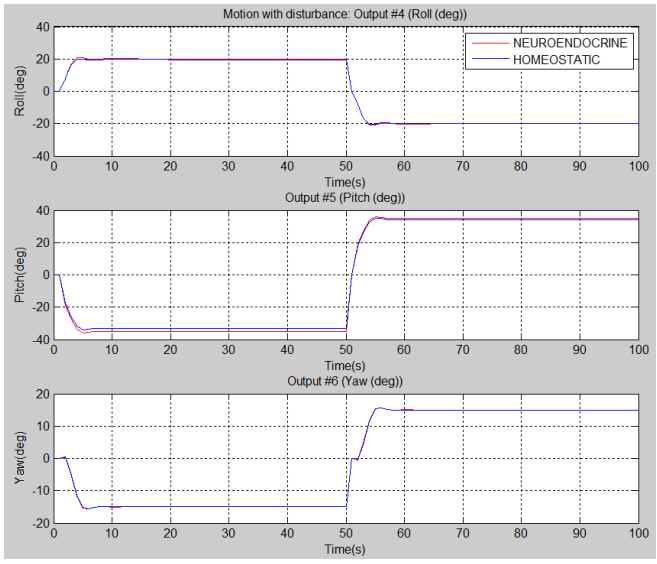

Figure 5. Euler angles

Fig. 5 shows that both controllers response converged to the desired Euler angles at the same settling time for all angles. However, the simulation results show that the homeostatic controller produced more accurate results than the neuroendocrine controller. Table I shows the comparison of the results between both controllers.

TABLE I. COMPARISON OF THE EULER ANGLES

Angles	Desired	Neuroendocrine	Homeostatic	Settling Time
Roll	20°	20.8171°	20.0982°	4s
Pitch	-35°	-35.9411°	-35.1460°	5s
Yaw	-15°	-15.2804°	-15.1805°	5s
Roll	-20°	-20.8171 °	-20.5328 °	4s
Pitch	35°	35.9411 °	35.1932 °	5s
Yaw	15°	15.2804 °	15.2786 °	5s

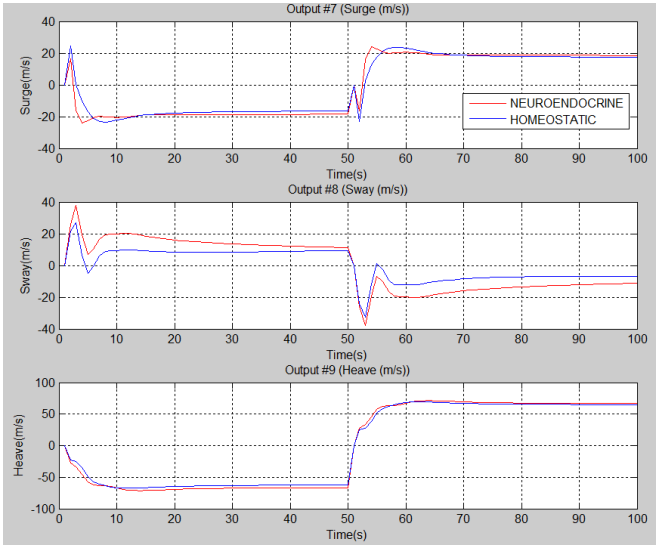

Figure 6. Translational velocities

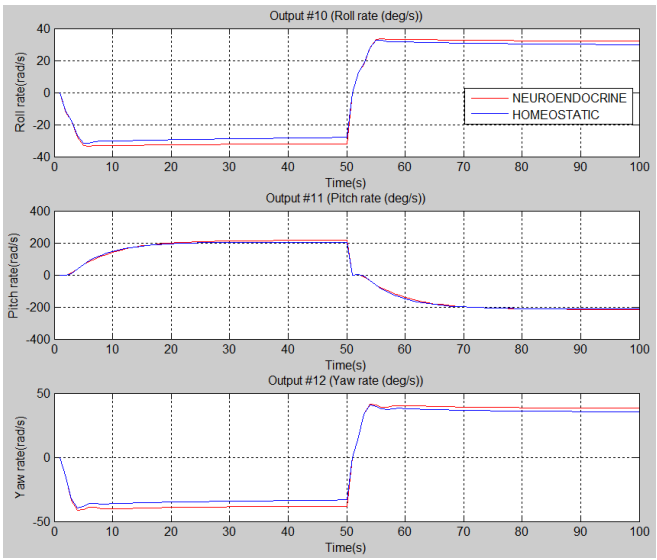

Figure 7. Angular velocities

Fig. 6 and 7 show the controller response for the glider translational and angular velocities, respectively. The graphs in both figures show that the velocity value of surge, u, sway, v, heave, w, roll rate, p, pitch rate, q and yaw rate, r for both controllers are slightly different. However, the homeostatic controller produced better control response than the neuroendocrine, especially for the surge velocity where the response was more stable than the neuroendocrine.

Fig. 8 shows the comparison of the response for the neuroendocrine and homeostatic controller over the position and forces of the sliding mass, and the mass of the ballast pump mass. The differences of the response for both controllers are obvious, where the homeostatic produced better control performance than the neuroendocrine because of the optimization process by the CSA in the AIS.

In order to achieve the desired pitch angle, the glider controls the sliding mass. Thus, to achieve -35° and 35° of pitch angle, the position of the sliding mass in x-direction for the neuroendocrine controller was determined as -44.5 cm and 44.5 cm, respectively. On the other hand, the position of the sliding mass in x-direction, r_{px}, for the homeostatic controller was determined as -37.2 cm and 38.7 cm, respectively. This observation shows that the required distance of the sliding mass to achieve both desired pitch angles has been shortened of 16.4% and 13%, respectively. This is because of the optimization process by the AIS in the homeostatic controller.

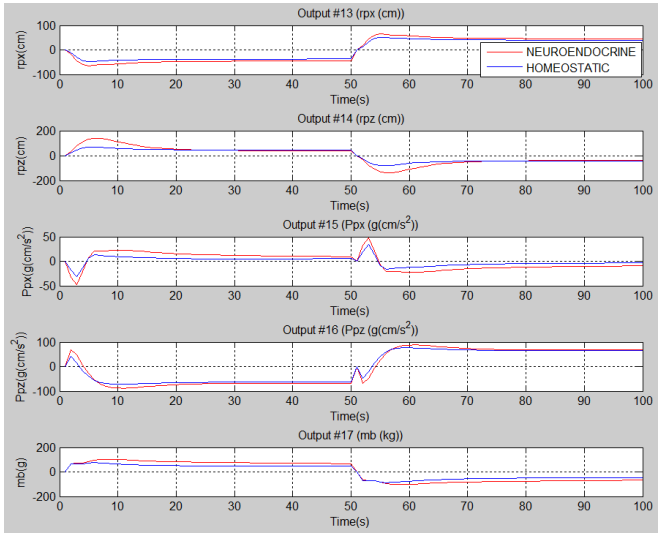

Figure 8. Position and forces of the sliding mass, and mass of the ballast pump

In order to analyse the effectiveness of homeostatic control system, we analysed and made a comparison of index performance's value (cost function) between the controllers in both motion conditions, as shown in Table II. The data shows that the homeostatic controller produced better performance with lower cost function than the neuroendocrine controller, and the optimization percentage was higher for the motion with disturbance than the motion without disturbance.

TABLE II. COMPARISON OF THE INDEX PERFORMANCE

Controller	Index performance for motion with disturbance	Index performance for motion without disturbance
Duration: 0-50s		
Neuroendocrine	8145.66	2918.94
Homeostatic	7571.89	2848.28
Optimization Percentage	7.04%	2.42%
Duration: 50-100s		
Neuroendocrine	8145.66	2918.94
Homeostatic	7786.46	2854.79
Optimization Percentage	4.41%	2.19%

V. CONCLUSION

The paper presents an analysis and a comparison between the homeostatic and neuroendocrine system for the motion control of the hybrid-driven underwater glider. The homeostatic control system is a connectionist of three artificial systems: artificial neural network (ANN), artificial endocrine system (AES) and artificial immune system (AIS). The backbone of the control system is the neural network. The MLP network architecture was used as the architecture of the neural network controller, which was designed to predict the control inputs as well as achieving the desired outputs. Meanwhile, the AES was designed to tune the weights of the neural network by secreting the hormone concentration from the artificial gland cell when the sensitivity of the weight was lower than zero, or the velocity of the water current was greater than zero. In order to select the best weight after the tuning process by the AES, the AIS is executed to optimize the controller by using the clonal selection algorithm (CSA).

In order to test the performance of the homeostatic control system, we have simulated the algorithm and tested it for different values of desired outputs. Referring to Table II, we found that the average of the index performance (cost function) for the homeostatic control system for the condition of the glider's motion with disturbance was 7679.18, and the average of the cost function for the neuroendocrine control system was 8145.66. This means that the cost function was reduced by 5.7%. On the other hand, the average of the cost function of the control system for the glider's motion without disturbance was reduced by 2.31%, where the average cost function of the homeostatic control system was 2851.54, and the average of the cost function of the neuroendocrine control system was 2918.94. Although the optimization percentage is considered low, the homeostatic controller algorithm was successfully optimized the glider's motion control system and produced better control performance.

ACKNOWLEDGMENT

The author would like to thank Malaysia Ministry of Higher Education (MOHE) ERGS-203/PELECT/6730045, Universiti Sains Malaysia (USM) and Universiti Tun Hussein Onn Malaysia (UTHM) for supporting the research.

REFERENCES

[1] R. Bachmayer, J. G. Graver, N.E. Leonard, "Glider control: a close look into the current glider controller structure and future developments", in Oceans 2003, pp. 951-954, 2003.

[2] D.C. Seo, G. Jo, H.S. Choi, "Pitching control simulations of an underwater glider using CFD analysis", in Oceans 2008, pp. 1-5, 2008.

[3] N. Mahmoudian, C. Woolsey, "Underwater glider motion control", in 47th IEEE Conference on Decision and Control, pp 552-557, 2008.

[4] N.E. Leonard, J.G. Graver, "Model based feedback control of autonomous underwater gliders", IEEE Journal of Oceanic Engineering, vol. 26, no. 4, pp. 633-645, 2001.

[5] K. Lei, Z. Yuwen, Y. Hui, C. Zhikun, "MATLAB-based simulation of buoyancy-driven underwater glider motion", Journal Ocean University of China, vol. 7, no. 1, pp. 133 - 188, 2008.

[6] Y. Wang, H. Zhang, S. Wang, "Trajectory control strategies for the underwater glider", in Int. Conference on Measuring Technology and Mechatronics Automation, pp. 918-921, 2009.

[7] B.H. Jun, J.Y. Park, F.Y. Lee, P.M. Lee, C.M. Lee, K. Kim, Y.K. Lim, J.H. Oh, "Development of the AUV 'ISiMI' and free running test in an ocean engineering basin", Journal of Ocean Engineering, vol. 36, no. 1, pp. 2-14, 2009.

[8] H. Yang, J. Ma, "Sliding mode tracking control of an autonomous underwater glider", in International Conference on Computer Application and System Modeling (ICCASM 2010), pp. 555-558, 2010.

[9] A. Budiyono, "Advances in unmmanned underwater vehicles technologies: modeling, control and guidance perspectives", Indian Journal of Geo-Marine Sciences, vol. 38, no. 3, pp. 282-295, 2009.

[10] A. Reza, A.A. Khayyat, K.G. Osgouie, "Neural networks control of autonomous underwater vehicle", in Int. Conference on Mechanical and Electronics Engineering (ICMEE 2010), vol 2, pp. 117-121, 2010.

[11] M. Neal, J. Timmis, "Timidity: A Useful Mechanism for Robot Control", Informatica, vol. 27, no. 4, pp. 197–204, 2003.

[12] T. Hoinville, P. Henaff, "Comparative Study of Two Homeostatic Mechanisms in Evolved Neural Controllers for Legged Locomotion", in IEEE/RSJ International Conference on Intelligent Robots and Systems, vol. 3, pp. 2624-9, 2004.

[13] P.A. Vargas, R.C. Moioli, L.N. De Castro, J. Timmis, M. Neal, F. von Zuben, "Artificial Homeostatic System: a Novel Approach", in the VIIIth European Conference on Artificial Life, pp. 754-64. 2005.

[14] R.C. Moioli, P.A. Vargas, F.J.V. Zuben, P. Husbands, "Evolving an Artificial Homeostatic System", in SBIA Joint Conference (SBIA), pp. 278-88, 2008.

[15] R.C. Moioli, P.A. Vargas, F.J.V. Zuben, P. Husbands, "Towards The Evolution of an Artificial Homeostatic System", in IEEE Congress on Evolutionary Computation (CEC), pp. 4024-31, 2008.

[16] K. Isa, M.R. Arshad, "Neural Network Control of Hybrid-Driven Underwater Glider", in Oceans 2012 MTS/IEEE-Yeosu, Conference and Exhibition, pp. 1-7, 2012.

[17] J. Timmis, M. Neal, J. Thorniley, "An adaptive neuro-endocrine system for robotic system", in IEEE Workshop on Robotic Intelligence in Informationally Structured Space, part of IEEE Workshops on Computational Intelligence, pp. 129-136, 2009.

[18] D. Dasgupta, "An overview of artificial immune systems and their applications", Springer, Berlin, 1998.

[19] L.N. De Castro, J. Timmis, "Artificial immune systems: a new computational intelligence approach", Springer, Heidelberg, 2002.

[20] J. Zheng, Y. Chen, W. Zhang, "A survey of artificial immune applications", Artificial Intell Review, vol. 34, no. 1, pp. 19-34, 2010.

[21] L.N. De Castro, F.J.V. Zuben, "The Clonal Selection Algorithm with Engineering Applications", in Workshop Proceedings of GECCO, Workshop on Artificial Immune Systems and Their Applications, pp. 36-37, 2000.

[22] L.N. De Castro, F.J.V. Zuben, "Learning and optimization using the clonal selection principle", IEEE Trans Evolut Comput, vol. 6, no. 3, pp. 239-251, 2002.